Modeling fast charge exchange recombination spectroscopy measurements from the Madison Symmetric Torus

S. Gangadhara,[a] D. Craig, D. A. Ennis, and D. J. Den Hartog
Center for Magnetic Self-Organization in Laboratory and Astrophysical Plasmas,
University of Wisconsin-Madison, 1150 University Avenue, Madison, Wisconsin 53706

Charge exchange recombination spectroscopy measurements of impurity ion temperature (T_i) and velocity (v_i) on the Madison Symmetric Torus present a unique challenge due to two coupled effects: low temperature—typically $300-500$ eV, though up to 2 keV in high current plasmas—and a dominant contribution from background, i.e., non charge exchange driven, emission. For low T_i, the background emission line shape is significantly asymmetric as a result of spin-orbit coupling effects. Accurate modeling of *both* the background and beam emission is therefore required to obtain precise values for local ion parameters. A model has been developed to provide robust simulation of the experimental measurements with ~ 10 μs temporal resolution using atomic data obtained from the Atomic Data and Analysis Structure database. Measurements are made using C VI emission at 343.4 nm, with background and beam emissions obtained simultaneously using two fiber bundles with slightly displaced lines of sight. Emission from O VI contributes substantially to the background signal, and is included in the modeling. A complete description of the model will be presented, along with results for T_i measurements during magnetic reconnection. © *2006 American Institute of Physics.* [DOI: 10.1063/1.2219412]

I. INTRODUCTION

Doppler spectroscopy is commonly used to determine ion velocity (v_i) and temperature (T_i) in laboratory and astrophysical plasmas. This technique involves measuring line radiation from plasma ions and extracting v_i and T_i from the centroid and width of the emission line shape, respectively. In general, measurements are made along the line of sight, yielding line-averaged values for the ion parameters. However, in many experiments active probing with a neutral beam is used to stimulate the emission, producing line radiation localized to the intersection volume between the beam trajectory and the measurement line of sight. This form of active spectroscopy is known as charge exchange recombination spectroscopy (CHERS) and has been employed for the diagnosis of high temperature plasmas for many years.[1,2] A system has recently been developed for the Madison Symmetric Torus (MST) reversed field pinch[3] (RFP) to allow fast, localized measurements of ion velocity and temperature using CHERS.[4] This system was designed to have spatial (~ 2 cm) and temporal (~ 10 μs) resolutions that permit a detailed study of the magnetohydrodynamic (MHD) dynamo[5] and ion heating during reconnection.[6,7]

II. EXPERIMENTAL SETUP

Localized values of the C^{+6} ion velocity and temperature are obtained on MST from measurements of C VI emission corresponding to the $n=7$ to $n=6$ transition in C^{+5} ($\lambda = 343.4$ nm). Emission is stimulated by charge exchange (CX) between hydrogen atoms injected radially into the plasma via a diagnostic neutral beam ($E=50$ keV) and fully stripped carbon ions in the background plasma. CX driven emission is concentrated along the beam path, since the cross section for charge exchange between C^{+6} and high-energy beam-injected neutrals is substantially larger than for charge exchange between C^{+6} and thermal background neutrals. Emission measurements are obtained from a set of views *perpendicular* to the beam, providing spatial localization. A cross section of MST showing the position of the beam and the measurement lines of sight is given in Fig. 1.

C VI emission may also be produced as a result of electron-impact (EI) excitation of background C^{+5} ions. Unlike radiation generated by charge exchange recombination, emission generated by electron-impact excitation is distributed over the plasma volume. Thus, along any line of sight that intersects the beam, both EI and CX driven emissions contribute to the measurement. However, for typical MST plasmas, the EI driven component is significantly larger than the CX driven component. Therefore, the dominant contribution to the measurement is from EI driven, i.e., background, radiation. Representative data shown in Fig. 2 illustrate this fact.

Emission data are obtained simultaneously using a pair of fiber bundles. For a given plasma discharge, these bundles are placed at a single view port, providing measurements from a single radial location. A total of 11 poloidal view ports are currently available on MST, as shown in Fig. 1. While one bundle views the beam directly—thus measuring both background (EI) and beam (CX) driven emissions—the other bundle is toroidally displaced so as to measure the
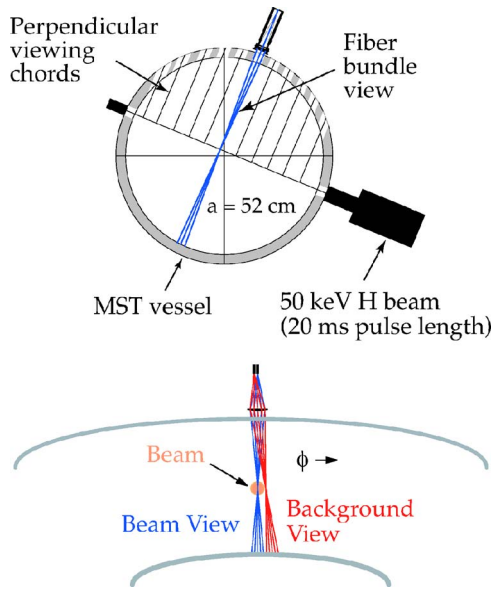
---

[a]Electronic mail: gangadhara@wisc.edu

FIG. 1. (Color online) Top: Cross section of MST showing the position of the diagnostic neutral beam and the views used to make CHERS emission measurements. Bottom: Schematic illustrating the position of the two fiber views, one looking directly at the beam (blue) and the other toroidally displaced to give a background measurement only (red).

FIG. 3. (Color online) Fine-structure components for the C VI line at 343.4 nm, for both charge exchange (bottom) and electron-impact excitation driven (top) emissions. Each curve represents the sum over all Doppler-broadened components.

background radiation only. The setup is shown schematically in Fig. 1. The fiber bundles are coupled to a custom-built grating spectrometer, which disperses light from each bundle over 16 wavelength channels. The dispersed light is collected in parallel by a 16×2 array of photomultiplier tubes, allowing fast data acquisition. Details on the system can be found in Ref. 4.

III. EMISSION MODEL

A. Effects of spin-orbit coupling

In many MST plasmas the ion temperature is low (200–500 eV), and emission modeling requires a detailed knowledge of the atomic structure of the emitting ion. The necessary data were obtained using the Atomic Data and Analysis Structure (ADAS) database,[8] and they indicate that for low T_i, effects of spin-orbit coupling are important. Spin-orbit coupling causes splitting of an otherwise degenerate emission line, as illustrated in Fig. 3, due to the interaction
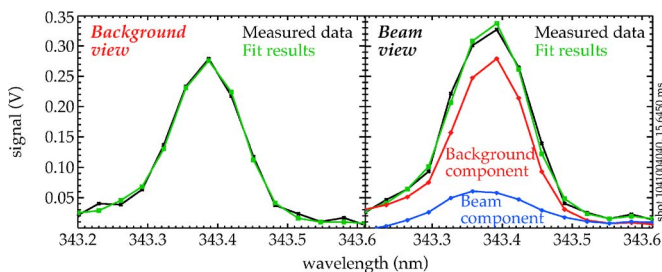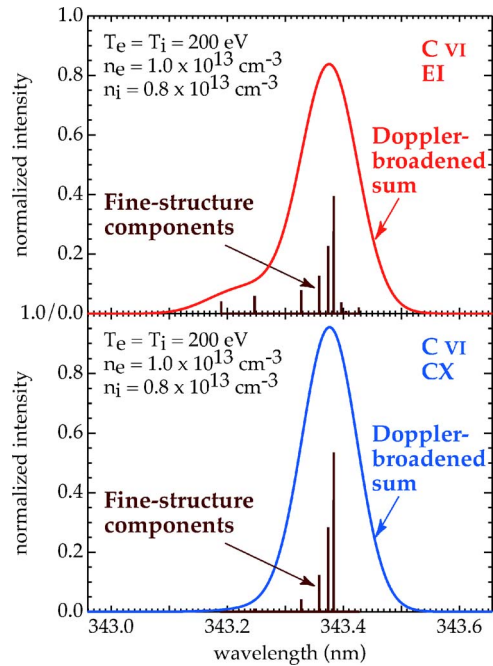

FIG. 2. (Color online) An example of typical C VI emission data and the corresponding fits. Fits are obtained using atomic data from the ADAS database and are shown in green in both panels. Left: Background (EI driven) emission measured along off-beam view. Right: Total (CX plus EI driven) emission measured along on-beam view. The contributions from charge exchange and electron-impact excitation are shown separately (red and blue, respectively).

between the orbital angular momentum and spin angular momentum of the electron. For the $n=7$ to $n=6$ transition in C^{+5}, the $\lambda=343.4$ nm line is split into 11 separate fine-structure components. The wavelength positions of the various components are fixed by the properties of the electronic transition, but the relative amplitude of each component is determined by properties of the background plasma, e.g., electron density and temperature. In addition, the relative amplitudes are different for transitions excited by electron-impact excitation and charge exchange recombination. This is illustrated in Fig. 3, where the fine-structure components for the CX and EI driven transitions are shown for $n_e = 10^{19}$ m^{-3} and $T_e=T_i=200$ eV. For emission produced by electron-impact excitation, the line shape develops an asymmetric tail due to contributions from low wavelength fine-structure components. Conversely, these components provide a negligible contribution to the charge exchange driven emission. However, since the on-beam measurement is dominated by background radiation, the experimental data are expected to be asymmetric, as observed in Fig. 2.

For a single emission line, Doppler broadening due to finite ion temperature produces a Gaussian line shape (assuming a Maxwellian distribution for the ions), and the centroid of the emission profile is Doppler-shifted from the vacuum wavelength due to finite ion velocity. In this case, a simple Gaussian fit to the data can be used to extract T_i and v_i as follows:

$$M = A_0 \exp[-(\lambda - \lambda_c)^2/2m_i\sigma^2], \tag{1}$$

$$v_i = c(\lambda_c - \lambda_0)/\lambda_0, \tag{2}$$

$$T_i = c^2(\sigma/\lambda_0)^2. \tag{3}$$

M is the simulated emission, used to model the measured data with the parameters A_0 (amplitude), λ_c (centroid), and σ (width). λ_0 is the vacuum wavelength for the emission line, c is the speed of light, and m_i is the mass of the emitting ion. When spin-orbit effects are included, each fine-structure component is Doppler broadened and Doppler shifted. The emission model is then more complicated, but similar in nature to Eq. (1):

For background (EI) data:

$$M_{EI} = A_{EI}\{\Sigma_j R_{j,EI} \exp[-(\lambda - \Delta\lambda_j - \lambda_{c,EI})^2/2m_i\sigma_{EI}^2]\}$$
$$+ B_0 + B_1\lambda, \tag{4}$$

and for total emission (CX+EI) data:

$$M_{TOT} = M_{EI} + M_{CX},$$

$$M_{CX} = A_{CX}\{\Sigma_j R_{j,CX} \exp[-(\lambda - \Delta\lambda_j - \lambda_{c,CX})^2/2m_i\sigma_{CX}^2]\}, \tag{5}$$

where j represents the fine-structure components ($j_{max}=11$). $R_{j,EI}$ is the relative amplitude of each of the EI components (normalized such that $\Sigma_j R_{j,EI}=1$) and $R_{j,CX}$ is the relative amplitude of each of the CX components (normalized such that $\Sigma_j R_{j,CX}=1$). $\Delta\lambda_j$ represents the known wavelength separation between the fine-structure components, which is calculated relative to the wavelength for the largest amplitude CX component.

For modeling the background data, there are five fitting parameters: $\lambda_{c,EI}$, used in Eq. (2) to find the line-averaged ion velocity; σ_{EI}, used in Eq. (3) to find the line-averaged ion temperature; A_{EI}, which is normalized such that $\int M_{EI}d\lambda =A_{EI}$, and thus provides a measure of the line-averaged C^{+5} brightness; and B_0 and B_1, which allow for the possibility of a baseline continuum emission in the measurement window that has both an offset ($=B_0$) and a slope ($=B_1$).

From Monte Carlo modeling it was found that for noisy signals with a significant background component, accuracy is improved by fitting the total emission data (which includes the background contribution) rather than subtracting the measured background emission from the total signal and fitting the residual (i.e., CX only) data. For a total signal level of N_{TOT} photons (typically $\sim$250–500) and a background-to-beam emission ratio of R_{BB} (typically $\sim$3–4), the fractional error goes as $1/\sqrt{N_{TOT}}$ for the total emission and as $\sqrt{[(2R_{BB}+1)\times(R_{BB}+1)]}/\sqrt{N_{TOT}}$ for the subtracted emission. These formulas, obtained using standard error propagation analysis and taking the signal noise to be governed by Poisson statistics, demonstrate the considerable increase in error for the subtracted signal when R_{BB} is large.

Modeling the total emission data requires three fitting parameters: $\lambda_{c,CX}$, used in Eq. (2) to find the local ion velocity; σ_{CX}, used in Eq. (3) to find the local ion temperature; and A_{CX}, which is normalized such that $\int M_{CX}d\lambda = A_{CX}$, and thus provides a measure of the local C^{+6} brightness. M_{EI} is determined from the fit to the measured background data and is given as an input to the total emission fit.
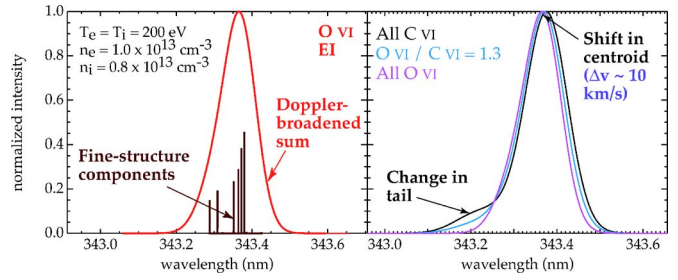

FIG. 4. (Color online) Left: Fine-structure components for the O VI line at 343.4 nm, for electron-impact excitation driven emission. The curve represents the sum over all Doppler-broadened components. Right: Variation of the background emission line shape with the O VI to C VI brightness ratio.

B. Role of oxygen in the background

Measurements of the local and line-averaged ion velocities have been made at a number of radial positions in MST, including on-axis. Equilibrium values for the on-axis velocity—both line-averaged and local—should be zero, since the line of sight is in the radial direction at this location. However, initial results for the line-averaged velocity yielded $v_i<0$. This was true for many different discharges, independent of background plasma conditions.

The results suggested the presence of additional (i.e., non-C VI) emission in the data. In fact, there exists an O VI line that corresponds to the $n=7$ to $n=6$ transition in O^{+5} with a wavelength of $\approx$343.4 nm. For typical MST conditions, the cross section for electron-impact excitation of the O VI line is approximately two orders of magnitude larger than the EI cross section for C VI. Thus, even for a small oxygen-to-carbon ratio in the plasma, the contribution of oxygen to the background emission is significant. ADAS was used to determine the fine-structure components for O VI, and the data are shown in Fig. 4. Also shown in this figure is a composite line shape profile for the background emission based on varying levels of oxygen to carbon. The presence of oxygen emission in the background signal produces two effects: a change in the shape of the low-wavelength tail and a shift of the profile centroid. The maximum shift corresponds to a velocity of $\sim$10 km/s, which is comparable to expected values for v_i. It is therefore necessary to include O VI in the background emission model, which is done by modifying Eq. (4) to include the O VI fine-structure components as follows:

$$M_{EI,CVI+OVI} = A_{EI}\{\Sigma_j R_{j,EI}$$
$$\times \exp[-(\lambda - \Delta\lambda_j - \lambda_{c,EI})^2/2m_C\sigma_{EI}^2]$$
$$+ \Sigma_k R_{k,EI} \exp[-(\lambda - \Delta\lambda_k$$
$$- \lambda_{c,EI})^2/2m_O\sigma_{EI}^2]\} + B_0 + B_1\lambda, \tag{6}$$

where j represents the fine-structure components for C VI (mass$=m_C$, wavelengths$=\Delta\lambda_j$) and k represents the fine-structure components for O VI (mass$=m_O$, wavelengths $=\Delta\lambda_k$, $k_{max}=15$). T_i and v_i are assumed to be equal for carbon and oxygen, which is valid since the ion-ion collision time between C^{+5} and O^{+5} is short compared to the measurement time scale. A renormalization is also performed so that $\Sigma_j R_{j,EI}+\Sigma_k R_{k,EI}=1$. Equation (6) contains the same number
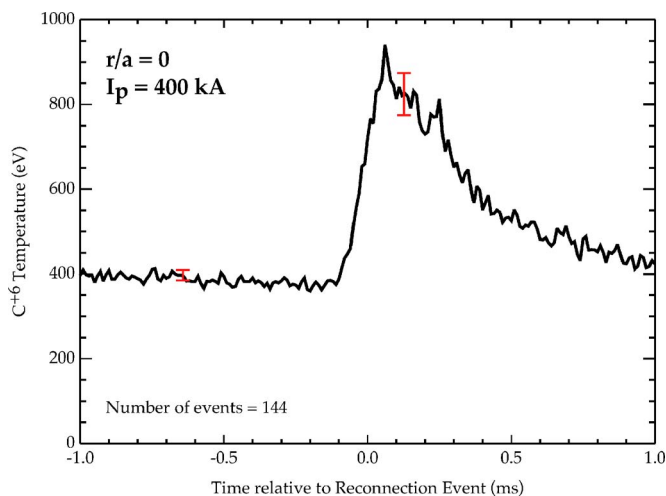
FIG. 5. (Color online) Measured evolution of the on-axis ion temperature through an impulsive reconnection event. The data represent an average over many similar events.

of fitting parameters as Eq. (4), and is used in the same manner to both fit the background emission and to provide a model of the background in the total emission fit.

The values $R_{j,\mathrm{EI}}$ in Eq. (6) represent the relative amplitudes of the C VI fine-structure components, whereas the values $R_{k,\mathrm{EI}}$ are the relative amplitudes of the O VI components *multiplied* by the ratio of the O VI to C VI brightness. The brightness ratio is determined from the measured data using the constraint that the line-averaged velocity be zero, and is typically $\approx 1-10$ for standard MST plasmas. During each experimental run day, the value for the O VI to C VI brightness ratio is obtained from initial on-axis measurements, and this value is assumed to remain constant for the entire day. Although this assumption may be tenuous, results for both the velocity fluctuations (used to calculate the MHD dynamo) and the ion temperature are, in fact, relatively insensitive to the value of the O VI to C VI brightness ratio, making it acceptable.

IV. DATA RESULTS

Model data generated using ADAS [i.e., Eqs. (5) and (6)] are convolved with the instrumental transfer functions of each measurement channel to construct simulated emission data. Simulated measurements are then compared to the ex-

perimental data and iterated upon until a best fit to the data is found, from which values for the line-averaged and local ion velocities and temperatures are obtained [using Eqs. (2) and (3)]. A comparison between simulated and experimental data is shown in Fig. 2. The results indicate good agreement, suggesting that ADAS provides an accurate model for the emission measurements.

A measurement of the on-axis ion temperature during an impulsive reconnection event is shown in Fig. 5. The data represent an average over a number of similar events. A large increase in T_i is observed, providing the first measurement of local ion heating during reconnection in the RFP. The heating occurs on a fast time scale, of order the reconnection time, while cooling occurs on a much slower time scale, of order the ion-ion collision time. Sample error bars are also shown in Fig. 5. Error bars are generated by fitting the experimental data obtained at each time point many times, in each case varying the emission data randomly within a range given by Poisson statistics. The range of temperature values extracted from the fits is used to calculate a mean and standard deviation, which provide the average value and the error bar for T_i, respectively.

[1] R. C. Isler and L. E. Murray, Appl. Phys. Lett. **42**, 355 (1983).
[2] R. J. Fonck, R. J. Goldston, R. Kaita, and D. Post, Appl. Phys. Lett. **42**, 239 (1983).
[3] R. N. Dexter, D. W. Kerst, T. W. Lovell, S. C. Prager, and J. C. Sprott, Fusion Technol. **19**, 131 (1991).
[4] D. Craig, D. J. Den Hartog, D. A. Ennis, S. Gangadhara, and D. Holly, Rev. Sci. Instrum. (submitted).
[5] D. J. Den Hartog, J. T. Chapman, D. Craig, G. Fiksel, P. W. Fontana, S. C. Prager, and J. S. Sarff, Phys. Plasmas **6**, 1813 (1999).
[6] E. Scime, S. Hokin, N. Mattor, and C. Watts, Phys. Rev. Lett. **68**, 2165 (1992).
[7] D. J. Den Hartog and D. Craig, Plasma Phys. Controlled Fusion **42**, L47 (2000).
[8] The original developer of ADAS is the JET Joint Undertaking, http://adas.phys.strath.ac.uk/